Figure 3(a) shows a temperature dependence of the fiber output and monitor current for one of the fabricated 50 samples of the plastic module. The fiber output was 0.2 mW in the full operating temperature range from −40–85°C. The monitor current was >100 μA at 0.2 mW fiber output and the tracking width of <+−20% was obtained in the full temperature range. The rise and fall time of the transmitter were <0.5 ns, which makes >622 MHz operation possible. These characteristics correspond to the conventional lower power version coaxial-type transmitter module. The thermal resistance of the plastic module was 100°C/W typical measured by wavelength-shifting method. Intermediate testing data shown in Fig. 3(b) indicate that the fiber output changes are <1 dB both for the heat cycling and 85°C/85% RH driving. These data indicate reliable operation of the fabricated plastic nonhermetic modules.

In conclusion, we have demonstrated high performance and small size plastic optical modules, which can be regarded as low-cost solutions for the optical transmitter module applying to the access network systems. The transfer molding packaging has advantages for the massive production like DRAMs than for pre-transfer molded housing. These two types of packaging will be selected by the results of reliability testing and the size of the application market. Reliability standards for the nonhermetic optical devices do not exist yet. The same sort of testing conditions for the nonhermetic packaged electronic LSIs used on the same circuit board of the optical devices, which satisfy Bellcore standard, can be proposed to be a reliability standard for the nonhermetic optical modules.

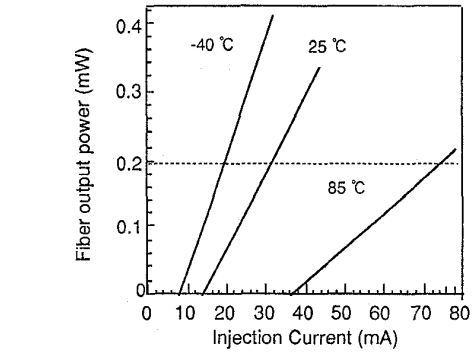

(a)

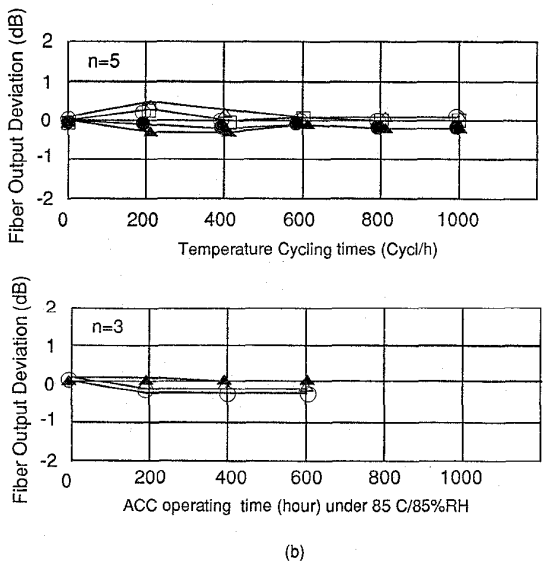

(b)

WB3 Fig. 3. Performance of the fabricated plastic module. (a) Temperature dependence of the plastic module fiber output and (b) Reliability testing operation for the heat cycling from −40°C to 85°C, and cw driving under 85°C/85% relative humidity.

1. S. Turley *et al.*, in *OECC'96*, p. 408.
2. J.V. Gates *et al.*, Proc. SPIE **2610**, 127 (1995).
3. K. Kurata *et al.*, presented at 6th International Workshop on Optical Access Networks, 1994, paper S 3.4-1.
4. K. Tatsuno *et al.*, in *OECC'96*, p. 408.
5. M. Shishikura *et al.*, in *OECC'96*, p. 458.
6. J.V. Collins *et al.*, Proc. SPIE **2610**, 108 (1995).

WB4 Invited 9:30am

An overview of micromachining for optical communications

Ming C. Wu, *UCLA, Electrical Engineering Department, 405 Hilgard Avenue, Los Angeles, California 90095-1594; E-mail: wu@ee.ucla.edu*

There have been increasing interests in applying the micromachining technologies to optical and optoelectronic systsm.[1] Despite the rapid advances of optoelectronic materials, optomechanical systems and mechanical actuation are still indispensable components in many optical systems for switching, display, printing, data storage, sensing, and packaging applications. The marriage of micro-optics and micromachining technologies has created a new family of optomechanical devices that cannot be realized by conventional technologies, and has opened up many new opportunities. Micromachining allows moveable as well as fixed optomechanical supporting structures to be integrated with optical and optoelectronic components. We review the state-of-the-art of the optical MEMS (micro-electro-mechanical-system) technologies around the world, and report on the recent progress of the free-space micro-optical bench (FSMOB) project at UCLA.

The optical MEMS technology has potential impace in several areas related to optical communications: optical switching, low-cost modulators, eavelength-division multiplexed (WDM) components, and packaging of optoelectronic components. In optical switching, MEMS provides a powerful tool to implement integrated optomechanical switches. The

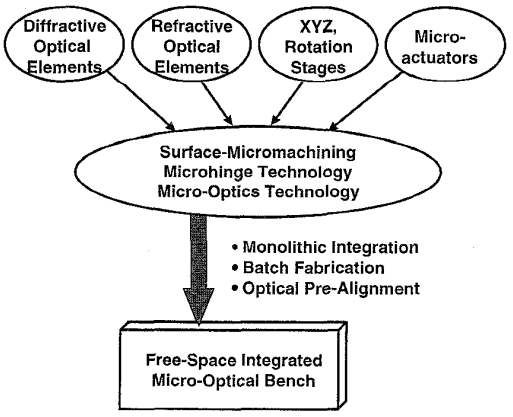

WB4 Fig. 1 The free-space micro-optical bench technology.

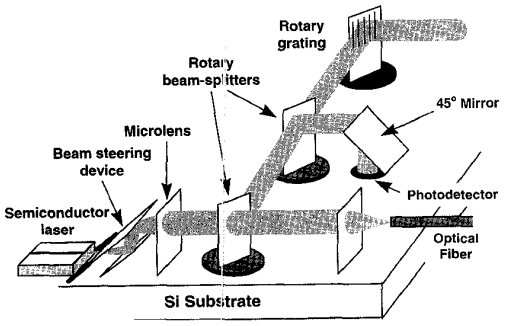

WB4 Fig. 2. Schematic diagram illustrating the concept of free-space micro-optical bench (FSMOB).

optomechanical switches have the advantages of very low insertion loss (<1 dB) and cross talk (<−50 dB). They are also independent of wavelength and polarization, transparent to modulation formats, and possibly require no standby power. Both free-space switches and guided-wave switches have been demonstrated. The guided-wave switch usually involves a moveable waveguide or moveable fiber. Very good performance has been demonstrated, however, it is usually not scaleable. The free-space approach expands the light from fibers into collimated beams. Switching is accomplished by moveable micromirrors in free space. An optical bypass switch for FDDI network and optical crossbar switches have been demonstrated. In the areas of optical modulators, low-cost reflection modulators have been demonstrated for upstream transmission in fiber-to-the-home applications. These devices typically employ a closely spaced Fabry–Perot (FP) resonant cavity structure. By moving one micromirror over a distance of a quarter wavelength, the reflectivity can be switched from high to low. Therefore, the device can function as a transmitter without requiring expensive lasers. The resonant frequencies of such devices are usually quite high (~ 1–10 MHz), and data rate up to 3.5 Mbit/s has been experimentally demonstrated. Display devices such as TI's digital micromirror devices and spatial light modulators' (SLM's) grating light valves can also be employed as SLM for optical interconnect and optical information processing. In WDM applications, tunable FP spectral filters with pass bandwidth of ~1 nm and tuning range in excess of 60 nm can be implemented. Such tunable filters can be monolithically integrated with photodetectors and vertical-cavity surface-emitting lasers in one epitaxial growth to form tunable lasers and photodetectors. The tuning ranges of such active optomechanical devices (> 20 nm continuously) are much larger than conventional devices.

Recent advances in surface-micromachining technology have further enabled the monolithic integration of free-space micro-optical elements, micropositioners such as XYZ stages and rotation stages, and microactuators on the same substrate (Fig. 1). This technique, called free-space miceo-optical bench (FSMOB), allows the entire free-space micro-optical system to be monolithically integrated on a single chip, as illustrated schematically in Fig. 2. Examples of such systems include free-space optical switches, optical disk pickup heads, microspectrometers, active laser-to-fiber couplers, and optical scanners. Details of optical MEMS fabrication technology, device and system performance, and the complete reference list will be given in the presentation.

1. See, for example, *Proceedings of IEEE LEOS Summer Topical Meeting on Optical MEMS and Their Applications* (Institute of Electrical and Electronics Engineers, New York, 1996).

WC

8:30–10:00am
Ballroom C3

Transmission Impairments
Robert Tkach, *AT&T Laboratories, Presider*

WC1 8:30am

Penalties induced by higher-order PMD at 10 Gbit/s in nondispersion-shifted fibers

F. Bruyère, L. Pierre, J.P. Thiery, B. Clesca, *Alcatel Alsthom Recherche, Rte. de Nozay, 91460 Marcoussis, France*

In a recently published work[1] (see also Ref. 2), we have demonstrated theoreticaly that in nondispersion-shifted fibers, second-order polarization-mode dispersion (PMD) can severely compound the PMD penalty as a result of first-order PMD [i.e., the value of the differential group delay (DGD) at the signal central frequency]. To verify these theoretical results, a 10-Gbit/s nonreturn to zero (NRZ) transmission was set up over a 70 km nondispersion-shifted fiber with a chromatic dispersion of +18 ps/nm.km near 1550 nm (Fig. 1). The 10-Gbit/s transmitter consisted of a 1557.557-nm distributed feedback (DFB) laser modulated by a $LiNbO_3$ Mach-Zehnder interferometer. Using a second DFB laser, tunable around λ_{peak} = 1557.557 nm and a HP8509B PMD analyzer, the DGD and PSP (principal states of polarization) characteristics of the fiber were measured over 20 GHz around λ_{peak} with a 2-GHz frequency step. Spatial switches at the fiber ends allowed alternation between (i) the measurement of the input power on the receiver for 10^{-10} bit-error-rate operation for the input polarization giving the worst penalty and (ii) the measurement of the DGD and PSP dependencies with the optical frequency.

Figure 2 shows the DGD dependency with the optical frequency offset from the signal center wavelength as well as a projection of the PSP variations on the Poincaré sphere in two cases yielding similar mean DGDs over 20 GHz (32.6 ps and 31.3 ps). The worst power penalty due to PMD (1.6 dB compared to 0.2 dB) was obtained for the case with the lower DGD at the signal central frequency (25.9 ps compared to 32.9 ps) but with the higher PSP rotation rate (14.2°/GHz compared to 3.3°/GHz). This result cannot be explained by first-order PMD theory, but is fully in accordance with the predictions of the theory including second-order PMD.[1]

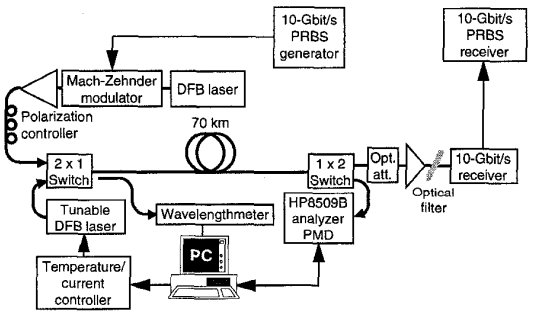

WC1 Fig. 1. Experimental setup used for 10-Gbit/s transmission and PMD monitoring over a 70-km G.652 nondispersion-shifted fiber.

Wednesday